Plaque disruption in a rabbit model of atherothrombosis occurs in regions of low endothelial shear stress

A. Phinikaridou[1], N. Hua[1], and J. A. Hamilton[1]
[1]Department of Physiology and Biophysics, Boston University, Boston, MA, United States

Introduction: Although the entire vasculature is exposed to the same systemic risk factors, local hemodynamic factors, in particular low endothelial shear stress (ESS), play a major role in the regional localization of atherosclerosis [1][2, 3]. In this study, we have employed *in vivo* MRI in a rabbit model of controlled plaque disruption to investigate whether the lowest values of ESS associate with the disruption of high-risk plaques and outward vessel wall remodeling.

Materials and Methods: Aortic atherosclerosis was induced in male New Zealand White (n=11) rabbits by cholesterol diet and endothelial denudation. Plaque disruption and thrombosis was induced with Russell's viper venom (0.15 mg/kg) and histamine (0.02 mg/kg) [4]. *In vivo* MRI of the abdominal aorta commenced before (pre) and after (post) the pharmacological triggering using a 3.0 T Philips Intera Scanner and a synergy knee coil with 6 elements. Axial T1-weighted black blood (T1BB) images were acquired with a double inversion recovery, turbo spin echo sequence and cardiac gating. The parameters for the TIBB images were: TR=2 cardiac cycles, TE=10ms, turbo factor=15, inversion delay = 350ms, slices = 23, slice thickness=4mm, NEX=2, MTX=384x362, reconstructed in-plane resolution=0.2x0.2 mm and scan duration=8min. Cardiac-gated, phase-contrast images were acquired with a 3D T1-fast-field echo sequence. The acquisition parameters were: TR=15.5ms, TE=6.8ms, slices = 23, slice thickness=4mm, NEX=2, MTX=208x158, reconstructed in-plane resolution=0.25x0.25 mm, flip angle=15^{o}, flow velocity=150 cm/s, cardiac phases=8-10, and scan duration=10 min. In addition, contrast-enhanced (CE), un-gated PC-MRA images were acquired with the same parameters described above but without the use of cardiac gating. Pre-triggered MRI images were used to calculate the plaque area, cross-sectional narrowing, ESS, and arterial remodeling. Plaque area and cross-sectional narrowing was calculated from T1BB images using ImageJ. The cardiac-gated PC-MRA images were used to calculate the ESS (dynes/cm) using an in-house Matlab software. The lumen was automatically segmented using a level set function [4]. The vessel wall was divided into 16 segments, which were determined at every 22.5° in the circumferential direction from the center of the mass. By averaging the cardiac cycle, the time averaged shear rates for 16 segments were calculated, the maximum of which was defined as the peak shear rate, while the mean was determined as the mean shear rate. The ESS was calculated as: Shear rate * viscosity (4 cPoise). The anatomical/flow compensated PC-MRA images were used to calculate the remodeling ratio [RR = vessel area $_{lesion}$/ vessel area $_{reference}$]. Three remodeling categories were defined: positive if RR>1.05, intermediate if 0.95 ≤ RR ≤ 1.05 and negative if RR <0.95 [5,6]. The post-triggered MR images were used to detect thrombi and classify plaques in stable (absence of thrombus) and vulnerable (presence of thrombus). All MRI assignments were validated histologically.

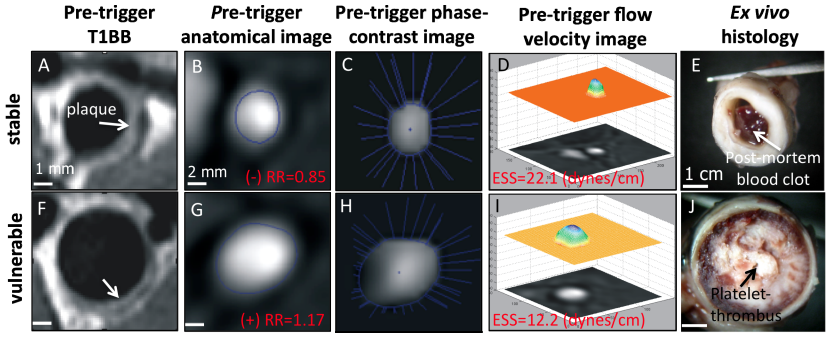

Results and Discussion: An example of the association between endothelial shear stress, vessel wall remodeling and plaque instability is illustrated in **Figure 1**. The pre-trigger T1BB images (**Fig.1A and 1F**) show a stable and a vulnerable plaque. The pre-trigger anatomical images (**Fig. 1B and 1G**) used to calculate the remodeling ratio show that the stable plaque underwent negative remodeling (RR=0.85) whereas the vulnerable plaque underwent expansive remodeling (RR=1.17). The pre-trigger phase contrast images (**Fig. 1C and 1H**) were used to derive the vectors associated with the magnitude of the ESS, at the contours outlined on the anatomical images (**Fig. 1B and 1G**). The magnitude of the ESS is illustrated in the surface plots (**Fig. 1D and 1I**) that indicate a higher ESS (22.1 dynes/cm) at the site of the stable plaque and a lower ESS (12.2 dynes/cm) at the site of the vulnerable plaque. *Ex vivo* histology verified the constrictive remodeling at the site of the stable plaque (**Fig. 1E**) and the expansion of the vessel wall at the site of the vulnerable plaque (**Fig. 1J**). Furthermore, Fig. 1J, reveals an occlusive platelet-rich thrombus associated with plaque disruption, whereas the clot seen at the site of the stable plaque is post-mortem coagulated blood. Statistical analysis of vulnerable (n=15) and stable (n=52) plaques revealed that vulnerable plaques cluster at regions with low mean ESS (12.2±1.5 vs. 18.5±2.7, *P*=0.001) and low peak ESS (33.2±5.4 vs. 70±20.6, *P*<0.001) compared to stable plaques. Bivariate analysis showed a significant negative correlation between peak ESS and plaque area (r=-0.34, *P*=0.001), and wall area (r=-0.57, *P*<0.001). Conversely, there was a positive correlation between peak ESS and cross-sectional narrowing (r=0.47, *P*<0.001). These data suggest that low ESS promotes plaque progression and outward remodeling, two major contributors of plaque instability. Logistic regression analysis revealed that peak ESS was an independent predictor of plaque disruption (P=0.02, OR=0.87, CI=0.78-0.98).

Conclusions: We demonstrated that low ESS is associated with plaques with positive arterial remodeling that disrupt after pharmacological triggering. Measurement of ESS by non-invasive MRI in individuals with atherosclerotic disease might be a useful parameter for assessing plaque instability and predicting the risk of future cardiovascular events.

References: **1**.Chatzizisis, Y.S., et al. J Am Coll Cardiol, 2007. 49(25): p. 2379-93. **2**.Caro, C.G., J.M. Fitz-Gerald, and R.C. Schroter. Nature, 1969. 223(5211): p. 1159-60. **3.** Chatzizisis, Y.S., et al. Circulation, 2008. 117(8): p. 993-1002. **4.** Chunming, L,. et al. IEEE Computer Society Conference, 2005. p. 430-436. **5.** Phinikaridou, A., et al. Circ Cardiovasc Imaging. 3(3): p. 323-32. **6.** Pasterkamp, G., et al. J Am Coll Cardiol, 1995. 26(2): p. 422-8.